Vol. 47, No. 4 (2025) 623-639, DOI: 10.24874/ti.1968.06.25.09

Tribology in Industry

www.tribology.rs

RESEARCH

Mathematical Modeling and Multi-Criteria Optimization in Dry Turning for Enhanced Functional Surface Using Bearing Area Curve

Amine Hamdi[a,*], Hammoudi Abderazek[b,c], Sidi Mohammed Merghache[a], Abdelhak Harouna[a], Tallal Hakmi[a]

[a]Laboratory of Mechanical Engineering, Materials and Structures, Tissemsilt University, 38000, Tissemsilt, Algeria,
[b]UR-MPE, M'hamed Bougara University, Independence Avenue, Boumerdes 35000, Algeria,
[c]Applied Precision Mechanics Laboratory, Institute of Optics and Precision Mechanics, Setif-1-University, Algeria.

Keywords:

Dry turning
functional surface
ISO 21920-2:2021
Pareto analysis
GRA
DF
RSM

* Corresponding author:

Amine Hamdi
E-mail : hamdi.amine@univ-tissemsilt.dz

Received: 24 June 2025
Revised: 7 August 2025
Accepted: 9 September 2025

A B S T R A C T

This research examines the parameters of the bearing area curve (BAC) as delineated by ISO 21920-2:2021 (R_{pk}, R_k, R_{vk}, $Mr1$, and $Mr2$), within the framework of dry turning of AISI 1045 steel (C45), to assess the impact of machining conditions on surface integrity. A combination of methodological tools is applied. Pareto analysis highlights the most significant machining factors: cutting speed (V_c), feed (f), depth of cut (ap), nose radius (r_ε), and principal cutting angle (X_r). Linear regression models are used to quantify the relationship between these variables and the BAC parameters. For multi-response optimization, both grey relational analysis (GRA) and the desirability function (DF) method from response surface methodology (RSM) are employed. The findings offer practical insights for improving surface finish by determining optimal cutting conditions. Specifically, the optimal setup includes a high cutting speed (420 m/min), low feed (0.031 mm/rev), maximum depth of cut (0.4 mm), large tool nose radius (0.8 mm), and low principal cutting angle (45°). The optimization yields a GRG of 0.773 and a stable DF value around 0.638, confirming the robustness and coherence of the proposed approach.

1. INTRODUCTION

Surface integrity, encompassing topographical, metallurgical, and micromechanical characteristics induced by machining, plays a key role in determining component performance, particularly in fatigue and stress corrosion resistance [1,2]. In this context, the bearing area curve (BAC), also known as the bearing ratio curve (BRC) or Abbott–Firestone curve (AFC), has emerged as a significant tool in surface metrology and tribology, enabling precise evaluation of surface roughness and contact regions by reflecting the influence of manufacturing processes [3,4]. According to ISO 21920-2:2021 [5], several parameters can be derived from this curve—R_k (core roughness depth), R_{pk} (reduced peak height), R_{vk} (reduced valley depth), $Mr1$ (peak material ratio), and $Mr2$ (valley material ratio)—which are extensively applied in automotive, aerospace, and industrial metrology to assess mechanical and tribological properties of machined surfaces, optimize lubrication, and reduce wear [6,7].

In machining processes, surface finish is a critical factor, particularly for high-precision mechanical components. Beyond its visual aspect, surface roughness directly affects the functional behavior of parts, influencing properties such as wear resistance, fatigue strength, and corrosion resistance [8,9]. Among the various material removal operations, turning holds a central role, as it is the most widely applied process in mechanical workshops. In this context, Abbas et al. [10] employed four multi-objective optimization algorithms to assess the effectiveness of dry turning of AISI 1045 steel (C45). Their findings indicated an average surface roughness (Ra) of 0.719 µm under the cutting conditions of feed (f) = 0.050 mm/rev, cutting speed (V_c) = 156.5 m/min, and depth of cut (ap) = 0.57 mm. In a subsequent study on the same material and process, the same author [11] demonstrated that wiper inserts significantly enhance machining performance, achieving a 67% increase in material removal rate compared with conventional inserts, while maintaining a surface roughness of about 0.7 µm. Furthermore, Szczotkarz [12] reported that an even higher surface quality can be attained in dry turning of AISI 1045 steel by employing titanium carbide (TiC)-coated tools, in combination with a feed f ≤ 0.15 mm/rev and cutting speed V_c > 225 m/min.

C45 steel (AISI 1045), well known for its favorable machinability across various chip-removal processes, is extensively used in mechanical engineering, particularly in the production of crankshafts, shafts, bolts, gears, and bearings [13,14]. The adoption of optimal cutting conditions is therefore a key factor for improving the efficiency of turning operations on this material in industrial applications [15]. In this regard, dry cutting trials were carried out to compare two coated carbides (GC4215-P15 and GC4225-P25) with an uncoated cermet (CT5015-P10) to evaluate flank wear. Using the response surface methodology (RSM), predictive models were developed and validated, highlighting the superiority of the GC4215 insert (100% efficiency), followed by GC4225 (98.4%) and CT5015 (83%) [16]. Overall, coated inserts demonstrated higher performance than uncoated ones in the machining of C45 steel [17]. However, in dry turning, flank wear of cermet inserts significantly reduced tool life, estimated at 35 minutes at 175 m/min and 23 minutes at 275 m/min for an average wear width of VB ≈ 0.1 mm [18]. Moreover, the deformation of C45 was found to decrease with increasing cutting speed (V_c), with a particularly sharp reduction observed between 145 and 180 m/min, and also tended to decline with higher feed [19]. Finally, when wiper carbide inserts were applied to the turning of AISI 1045, an average surface roughness of Ra = 0.202 µm was achieved under the conditions V_c = 80 m/min, ap = 0.5 mm, and f = 0.045 mm/rev, with a relative error below 3% [20].

While traditional roughness parameters provide a first-level geometric description, they show certain limitations. Therefore, they are often complemented by functional parameters derived from the Abbott-Firestone curve. Although numerous studies have examined the dry machining of C45 steel (AISI 1045), particularly with regard to surface integrity characterization, investigations specifically addressing the five-bearing area curve (BAC) parameters remain scarce, if not nonexistent. Yet, these indicators — R_{pk}, R_k, R_{vk}, $Mr1$, and $Mr2$ — are critical for evaluating the functional performance of machined surfaces, as they provide key insights into wear resistance and the load-bearing capacity of mechanical components.

In this context, the primary objective of the present work is to investigate the impact of five input parameters (V_c, f, ap, r_ε, and X_r) in the dry turning of C45 steel, with the aim of minimizing R_{pk}, R_k, and $Mr1$, while maximizing R_{vk} and $Mr2$, in order to enhance the functional quality of machined surfaces. The adopted methodology involves three main stages: Identifying the most influential factors affecting the responses using Pareto charts and 3D response surface plots, modeling and validating the responses through Response Surface Methodology (RSM), and optimizing the process using two multi-objective approaches: Grey Relational Analysis (GRA) and Desirability Function (DF).

2. MATERIALS AND METHOD

2.1 Workpiece material

C45 steel (AISI 1045) was utilized as the workpiece material in the experimental investigations. The workpiece exhibited a Brinell hardness of 150 HB. The measurement was conducted directly on the sample surface through three repetitions. The diameter of specimens is 65 mm and length of 250 mm, each sample contained eight grooves, each measuring 5 mm in width and spaced 20 mm apart. This steel is widely used in various industrial applications [21]. Table 1 presents the mechanical properties and chemical composition of the C45 steel specimens.

Table 1. Chemical composition of C45 steel.

Mechanical properties	Yield strength 370 MPa		Tensile strength 675 MPa		Elongation A 15.67 %	
Elements	C	Si	Mn	P	S	Cr
Wt. (%)	0.43	0.39	0.72	0.04	0.02	0.32

2.2 Machine tools and equipment

The conventional lathe "LMO Microweily TY-1640S" was used for the dry turning of the C45 steel specimens. In this regard, the inserts employed were SNMG 120404 (nose radius, $r_\varepsilon = 0.4\,mm$) and SNMG 120408 (nose radius, $r_\varepsilon = 0.8\,mm$). Two tool holders were employed for mounting the inserts: PSBNR 2525 M12 (tool cutting edge angle, $X_r = 75°$) and PSSNR 2525 M12 (tool cutting edge angle, $X_r = 45°$). Dry turning was carried out using a fresh cutting edge for each experiment in order to eliminate any potential influence of tool wear on the BAC parameters. This approach also ensures consistent and reproducible cutting conditions throughout the experimental campaign. Figure 1 illustrates the experimental setup used to collect the response data for the BAC. The selection of inserts and tool holders was guided by technical, geometrical, and economic criteria. Square-shaped SNMG inserts provide eight reusable cutting edges, ensuring higher cost-effectiveness at the same price. The tool holders were chosen for their compatibility with SNMG inserts, their structural robustness, and their ability to accommodate two main cutting angles suitable for the experimental conditions.

A Mitutoyo Surftest SJ-310 profilometer was used to gather experimental data pertaining to the Abbott-Firestone curve. The device has a stylus with a 2 μm tip radius, proficient at identifying subtle surface abnormalities. In compliance with ISO 12085, the analysis used a Gaussian cutoff filter and a sample length of 0.8 mm, yielding an assessment length of 4 mm [22]. Three measurements were taken on distinct surface zones, spaced 120°. The mean value was used for analysis. If one measurement deviated by more than 5% from the mean of the other two, it was treated as an outlier and discarded, and the measurement was repeated until three consistent values were obtained (all within 5% of the mean).

2.3 Experimental design

We used the Taguchi approach in this study to minimize the number of experiments and stay within the allocated budget. This comprehensive statistical methodology for design of experiments (DoE) allows for improved product and process quality by reducing susceptibility to fluctuations and external noise causes. We apply optimal experimental designs and optimize the signal-to-noise ratio (S/N) to achieve enhanced performance using fewer resources. This approach is widely used in various fields, including the examination of tribological excellence [23], tribological Performance [24], and the machining of unreinforced polymers [25].

In this stage, the control factors and their respective levels were selected, as shown in Table 2. Four levels were defined for the conventional cutting parameters: cutting speed, feed, and depth of cut. Additionally, two levels were selected for the cutting tool parameters: nose radius and principal cutting-edge angle. Therefore, the total number of experiments required for a full factorial design ($4^3 \times 2^2$) amounts to 256 experiments, whereas the Taguchi method requires only 16 experiments using an L_{16} orthogonal array, as presented in Table 3. The levels of the control factors were determined based on the recommendations of the company Sandvik Coromant, the manufacturer of the cutting inserts, and the producer of the low-alloy steel AISI 1045.

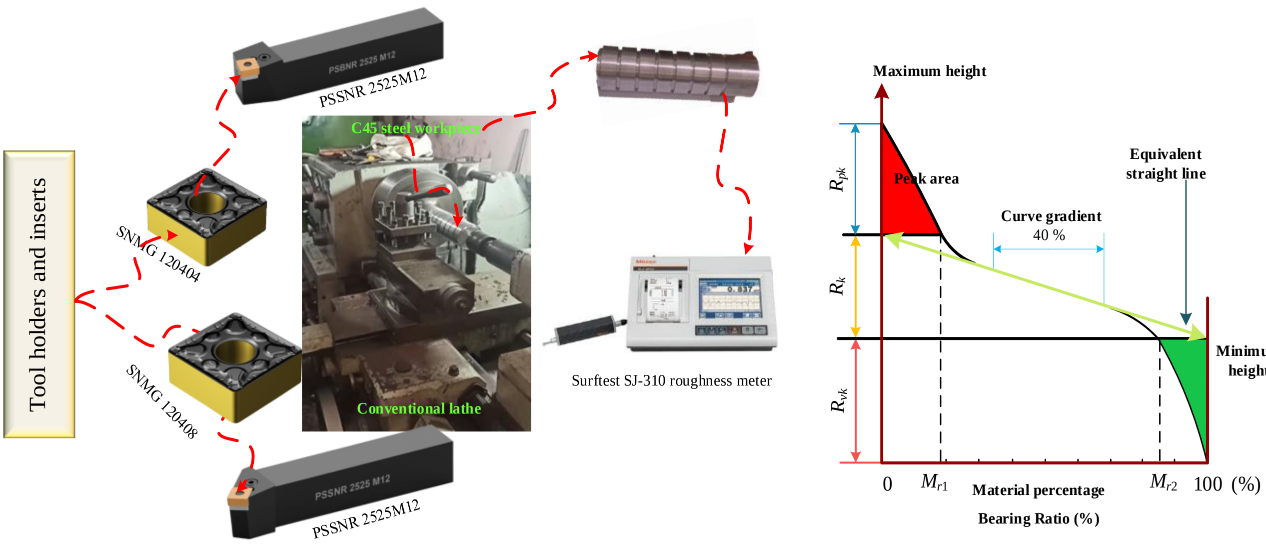

Fig. 1. Dry turning experimental stage and data acquisition process.

Table 2. Control factors and their levels.

N°	Processing factors				
	V_c (m/min)	f (mm/rev)	ap (mm)	r_ε (mm)	X_r (°)
1	80	0.031	0.1	0.4	45
2	185	0.062	0.2	0.8	75
3	270	0.124	0.3	–	–
4	420	0.248	0.4	–	–

3. RESULTS AND DISCUSSION

3.1 Experimental results

Table 3 presents the experimental results for the material ratio curve (MRC) parameters (R_{pk}, R_k, R_{vk}, $Mr1$, and $Mr2$) as a function of the cutting parameters and tool geometry (V_c, f, ap, r_ε, and X_r). The measured MRC parameters are consistent with the manufacturers' recommendations, confirming that the machined surfaces comply with industrial specifications [26].

Analysis of the data in this table reveals a significant correlation between the cutting conditions and the resulting surface quality. A high cutting speed (V_c = 420 m/min) notably reduces the reduced peak height (R_{pk} = 1.2 µm), the core roughness depth (R_k = 2.5 µm), and the reduced valley depth (R_{vk} = 1.02 µm), contributing to a smoother surface with improved functional contact. Conversely, a high feed rate (f = 0.248 mm/rev) and a large depth of cut (ap = 0.4 mm) tend to increase roughness, thereby deteriorating surface quality, as evidenced by Trial 4 where R_{pk} = 6.78 µm, R_k = 13.1 µm, and R_{vk} = 4.5 µm. Moreover, the influence of the tool nose radius (r_ε = 0.8 mm) is critical: a larger radius enhances surface finish by reducing cutting aggressiveness and distributing cutting forces more evenly. Finally, a higher principal cutting edge angle (X_r = 75°) appears to improve the material ratio, promoting better tool–material contact and reducing wear, as shown in Trial 16 with a material ratio in the peak zone ($Mr1$ = 25.62%) and valley zone ($Mr2$ = 97.67%). For all 16 experiments, the values of R_k exceed those of R_{pk} and R_{vk}, which contributes to enhanced wear resistance of the inner cylinder surfaces, as noted by Buj-Corral et al. [6].

3.2 Pareto analysis

This tool is particularly useful for identifying the most influential factors and prioritizing process improvement actions. A reference line at 0.05 (α = 5%) is included to indicate statistically significant effects. Displaying the absolute values of the effects, the chart helps to highlight the most impactful factors, although it does not indicate whether they increase or decrease [27,28].

The Pareto chart presented in Fig. 2 highlights the relative impact of the different machining factors on the reduced peak height (R_{pk}). With a Pareto coefficient α = 2.23 and a given significance level, the statistical analysis identifies the variables with a predominant influence on this parameter.

Thus, factors whose effects exceed the red line are considered statistically significant, while those below the line are not. Additionally, certain parameters, such as f and V_c, exhibit a dominant effect, meaning they play a key role in improving surface quality. In this analysis, feed f has the most significant effect, followed by speed V_c and the angle (X_r), which should be prioritized to optimize the process. In contrast, DoC (ap) and nose radius (r_ε) have a negligible influence.

Table 3. Experimental results.

Trail n°	V_c (m/min)	f (mm/rev)	ap (mm)	r_ε (mm)	X_r (°)	R_{pk} (μm)	R_k (μm)	R_{vk} (μm)	$Mr1$ (%)	$Mr2$ (%)
1	80	0.031	0.1	0.4	45	2.86	8.93	5.29	8.29	87.73
2	80	0.062	0.2	0.4	45	3.22	8.57	4.70	7.70	88.40
3	80	0.124	0.3	0.8	75	5.46	12.14	4.20	9.70	92.49
4	80	0.248	0.4	0.8	75	6.78	13.10	4.50	8.98	93.80
5	185	0.031	0.2	0.8	75	2.93	9.66	5.20	7.90	87.20
6	185	0.062	0.1	0.8	75	3.62	11.20	5.43	10.70	88.70
7	185	0.124	0.4	0.4	45	3.43	5.96	2.34	8.08	93.40
8	185	0.248	0.3	0.4	45	6.50	8.51	2.01	16.40	97.10
9	270	0.031	0.3	0.4	75	2.42	6.08	3.02	7.95	90.22
10	270	0.062	0.4	0.4	75	2.78	5.61	2.43	9.95	91.83
11	270	0.124	0.1	0.8	45	3.40	8.30	3.44	8.98	91.70
12	270	0.248	0.2	0.8	45	4.50	7.50	2.30	14.48	96.48
13	420	0.031	0.4	0.8	45	1.20	2.50	1.50	3.90	92.59
14	420	0.062	0.3	0.8	45	1.33	3.02	1.29	7.08	93.10
15	420	0.124	0.2	0.4	75	3.01	3.92	1.22	18.56	94.04
16	420	0.248	0.1	0.4	75	5.66	8.80	1.02	25.62	97.67

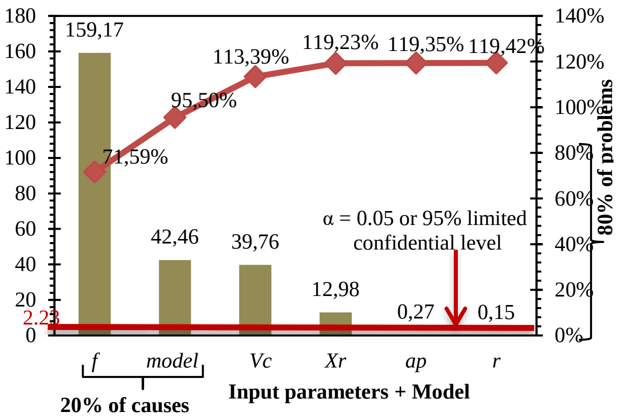

Fig. 2. Pareto chart for the reduced peak height R_{pk}.

The Pareto chart in Fig. 3 analyzes the influence of machining parameters on the R_k, a key criterion for assessing surface quality, as it represents the height of the primary irregularities remaining after machining. As with the response R_{pk}, the investigated factors include cutting speed, feed rate, depth of cut, tool nose radius, and cutting angle. In this diagram, the bars illustrate the relative impact of each factor on R_k, while the significance line indicates the threshold for statistical significance. When certain parameters such as V_c or X_r, exceed this threshold, they are identified as the primary contributors to variations in R_k.

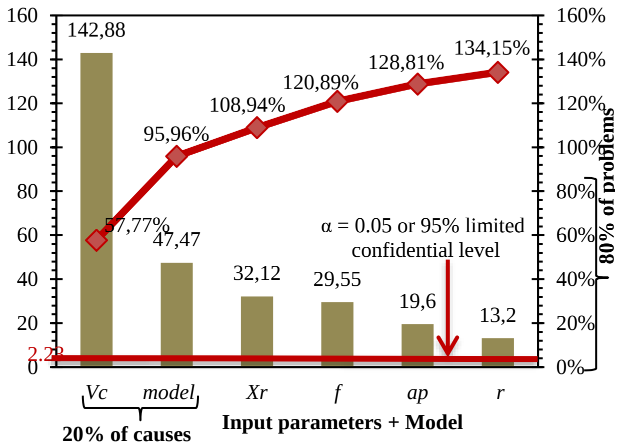

Fig. 3. Pareto chart for the core roughness depth R_k.

The Pareto chart in Fig. 4 illustrates the influence of machining parameters on the R_{vk}. Unlike R_{pk} and R_k, where minimization is desirable, a high R_{vk} value is sought to enhance lubricant retention capability and wear resistance of machined surfaces. Taller bars indicate factors with a major impact, while the significance line identifies those that statistically influence this parameter. In this control chart, all factors are statistically significant, as each bar exceeds the reference line set at 2.57%. In this case, the input parameters are ranked in descending order of impact: V_c, f, ap, r_ε, and X_r.

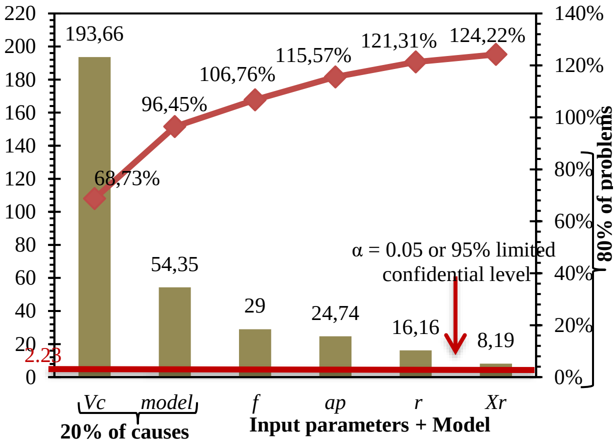

Fig. 4. Pareto chart for the reduced valley depth R_{vk}.

Figure 5 shows the Pareto chart of the material ratio in the peak zone ($Mr1$). This measure is crucial for characterizing the surface condition of machined components, particularly regarding their load-bearing capacity and wear resistance. A minimal $Mr1$ value is advantageous for enhancing surface quality, as it reflects lower peak heights, facilitating more uniform contact and increasing mechanical strength.

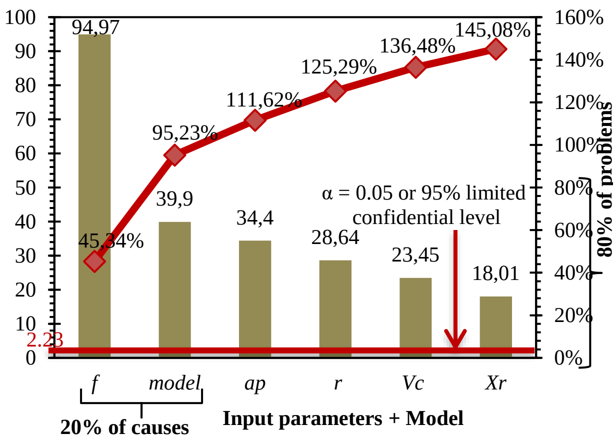

Fig. 5. Pareto chart for the peak material ratio $Mr1$.

The tallest bars indicate the most substantial effects, while the significance line delineates the factors with statistically significant impact. All parameters surpass the threshold line, signifying their impact on variations in peak roughness. An analysis of the chart facilitates the optimization of machining conditions to reduce $Mr1$. f is a significant and positively correlated factor; thus, its reduction may result in a more uniform surface and improved wear resistance. An optimal adjustment of ap may limit the formation of excessive peaks, thus enhancing the final surface quality.

Figure 6 presents a Pareto chart, illustrating the effect the machining parameters on the material ratio in the valley zone ($Mr2$). This parameter is significant as it indicates the capacity of a machined surface to retain lubricants and withstand wear. A higher $Mr2$ value is generally preferred, as it indicates the surface's capacity to retain more lubricant, thereby reducing friction and wear and enhancing the surface's tribological performance. The tallest bars represent the parameters with the most substantial impact, whereas the dashed line indicates the effects that are statistically significant. In this regard, the f, V_c, and ap exceed the threshold line, indicating their key role in influencing $Mr2$ variations. A detailed analysis of the chart allows for the optimization of machining conditions to maximize $Mr2$. Moreover, since feed is the dominant factor, a precise adjustment may be necessary to achieve a more functionally effective surface. The predominance of feed (f) and speed (V_c) is explained by their direct physical influence: feed governs chip thickness and peak formation (R_{pk}, R_{pk}, and $Mr1$)), while cutting speed controls heat generation and chip flow, thereby affecting valley depth and lubricant retention (R_{vk} and $Mr2$). These mechanisms justify why f and V_c consistently dominate in the Pareto analysis.

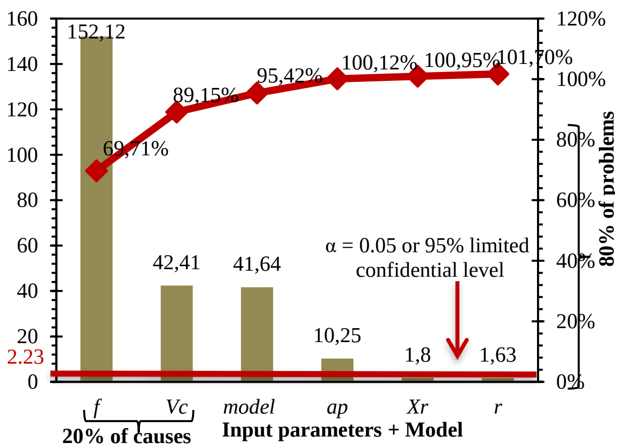

Fig. 6. Pareto chart for the valley material ratio $Mr2$.

3.3 Linear regression

Linear regression is a statistical method used to model the relationship between a dependent (or response) variable (Y) and one or more independent (or explanatory) variables (X_i). It is based on the assumption that this relationship can be approximated by a linear function. In this context, the technique is widely used across various fields such as CNC machining evaluation [29], honing [30], steel turning [31], plasma jet cutting [32].

Equation 1 describes the relationship to reduce the peak height R_{pk}. The mathematical model takes into consideration 95.5% of the variance in R_{pk}, with 4.5% remaining unexplained.

$$R\_pk = 1.789 - 0.00547V\_c + 6.38f - 0.5a\_p - 0.206r\_\varepsilon + 0.02592X\_r \quad (1)$$

$$(R^2_{R_{pk}} = 95.50\%)$$

Equation 2 delineates the linear model used for the regression of core roughness depth R_k. The coefficient of determination is 95.96%, indicating that the model explains for this percentage of the variation in R_k, with 4.04% remaining unexplained.

$$R_k = 6.15 - 0.01825V_c + 12.42f - 7.52a_p + 3.45r_\varepsilon + 0.0717X_r \quad (2)$$

$$(R^2_{R_k} = 95.96\%)$$

Equation 3 describes the linear relationship used to model the reduced valley depth, denoted as R_{vk}. The model explains 96.45% of the variance in this response, leaving 3.55% unexplained.

$$R_{vk} = 5.099 - 0.01013V_c - 5.87f - 4.033a_p + 1.822r_\varepsilon + 0.0172X_r \quad (3)$$

$$(R^2_{R_{vk}} = 96.45\%)$$

Equation 4 defines the linear model for the upper limit position of the core roughness profile, denoted as $Mr1$. The coefficient of determination (R^2) is 95.23%, indicating that this proportion of the variance in $Mr1$ is explained, leaving 4.77% unexplained.

$$Mr1 = 7.03 + 0.01401V_c + 42.22f - 18.89a_p - 9.63r_\varepsilon + 0.1019X_r \quad (4)$$

$$(R^2_{Mr1} = 95.23\%)$$

Equation 5 defines the linear model for the lower limit position of the core roughness profile, denoted as $Mr2$. The coefficient of determination is 95.42%, meaning that the model explains this proportion of the variance in $Mr2$, while 4.58% remains unexplained.

$$Mr2 = 86.41 + 0.01108V_c + 31.43f + 6.06a_p - 1.35r_\varepsilon - 0.019X_r \quad (5)$$

$$(R^2_{Mr2} = 95.42\%)$$

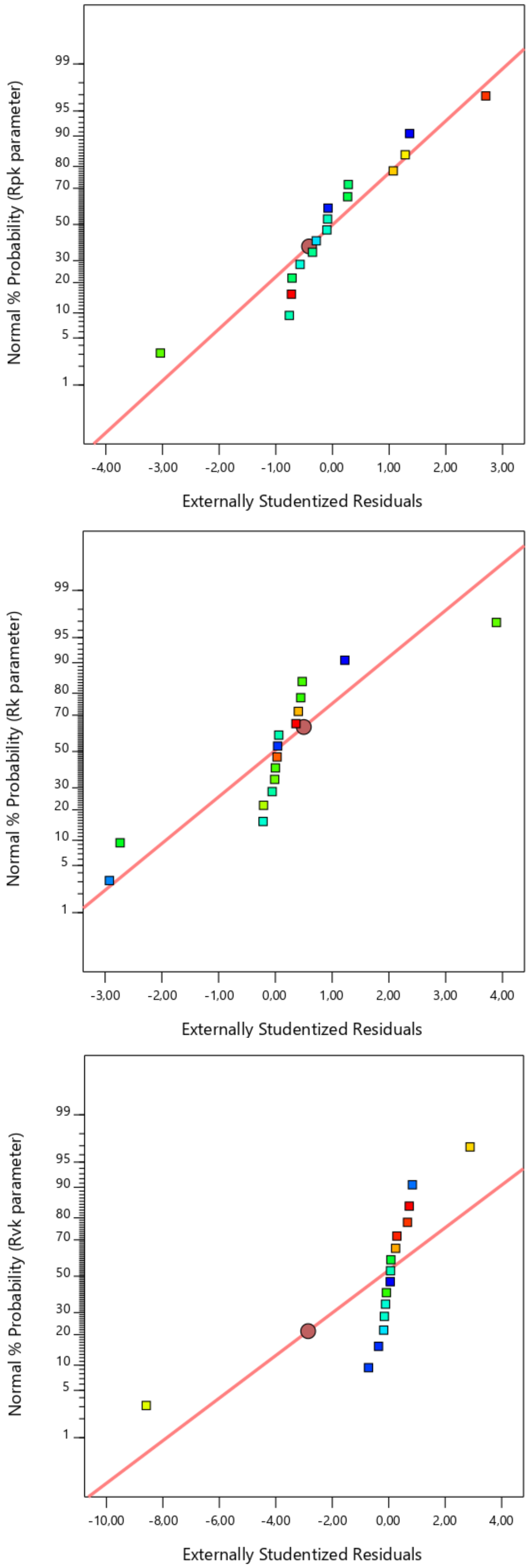

Fig. 7. Normal graphs of residuals from responses R_{pk}, R_k, and R_{vk}.

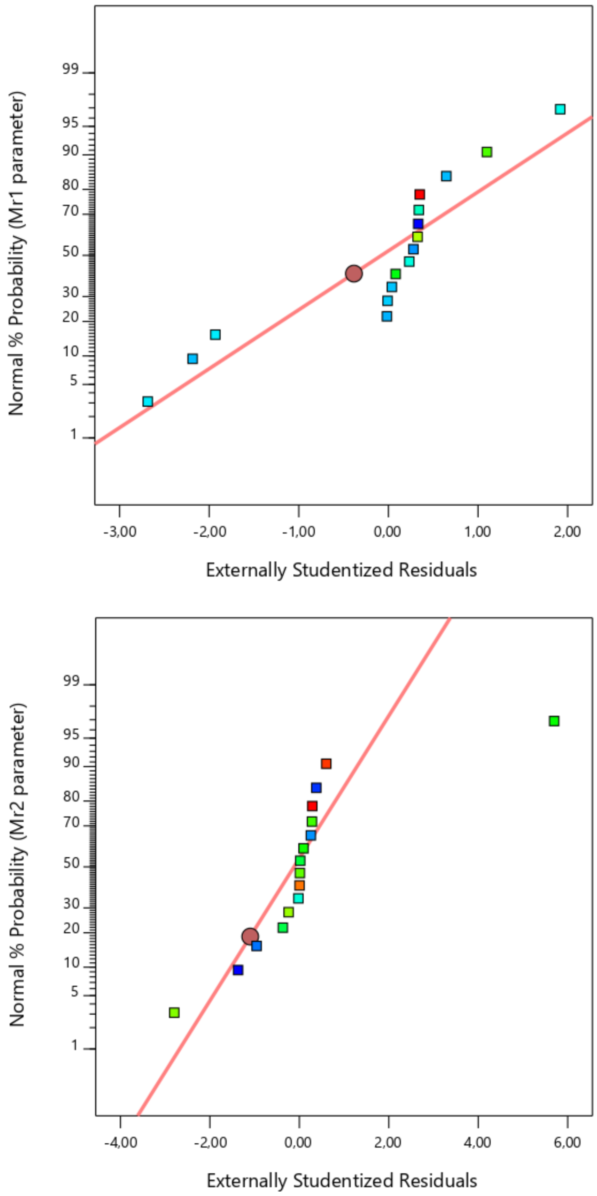

Fig. 8. Normal graphs of residuals from responses $Mr1$, and $Mr2$.

The analysis of the normal probability plots of residuals for the parameters R_{pk}, R_k, R_{vk}, $Mr1$, and $Mr2$, presented in Figures 7 and 8, shows that the points generally align well with the reference line, indicating an approximately normal distribution of residuals. This consistency confirms that the normality assumptions underlying the applied statistical models are largely satisfied, thereby strengthening the reliability and validity of the obtained results. Minor deviations observed at the tails, particularly for R_{pk} and R_{vk}, suggest a slight asymmetry in the distribution; however, these do not compromise the robustness of the models.

3.3.1 Comparison between experimental and predicted results

The analysis of Figs. 9 and 10 highlights the agreement between the experimental values, represented by blue dots, and the predicted values, illustrated by a red linear trendline, for the various studied responses.

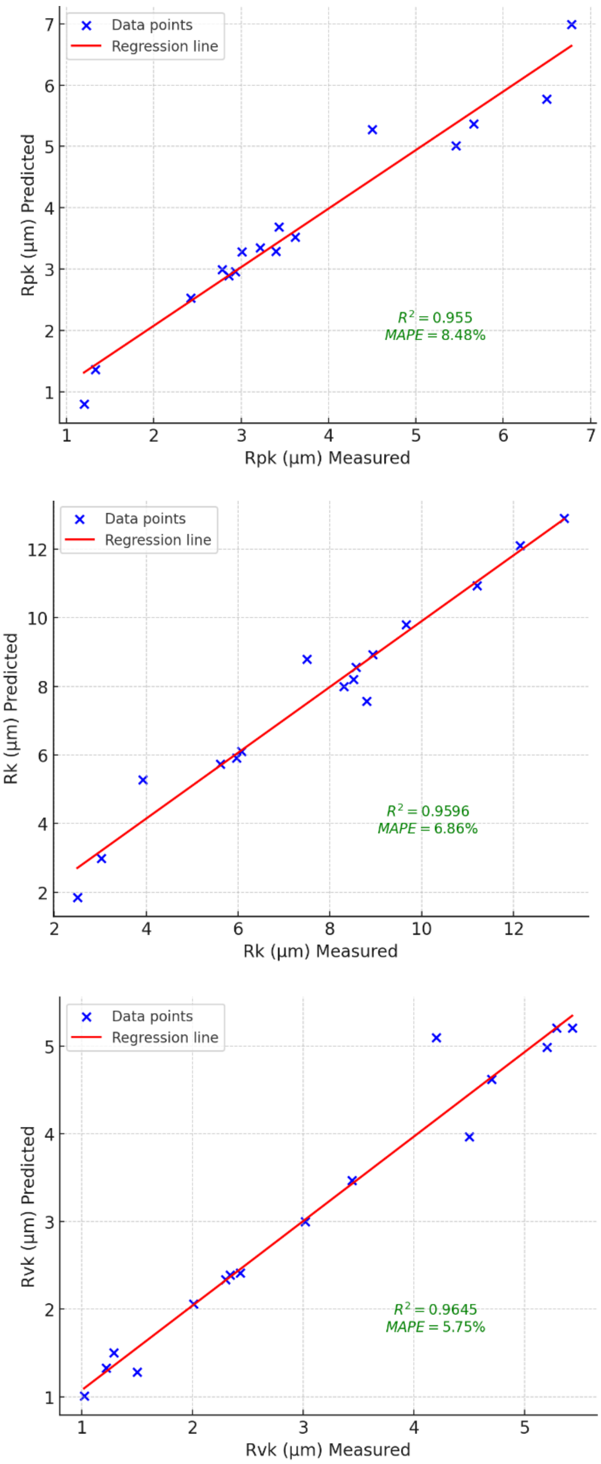

Fig. 9. Experimental and predicted results for R_{pK}, R_k, and R_{vk}.

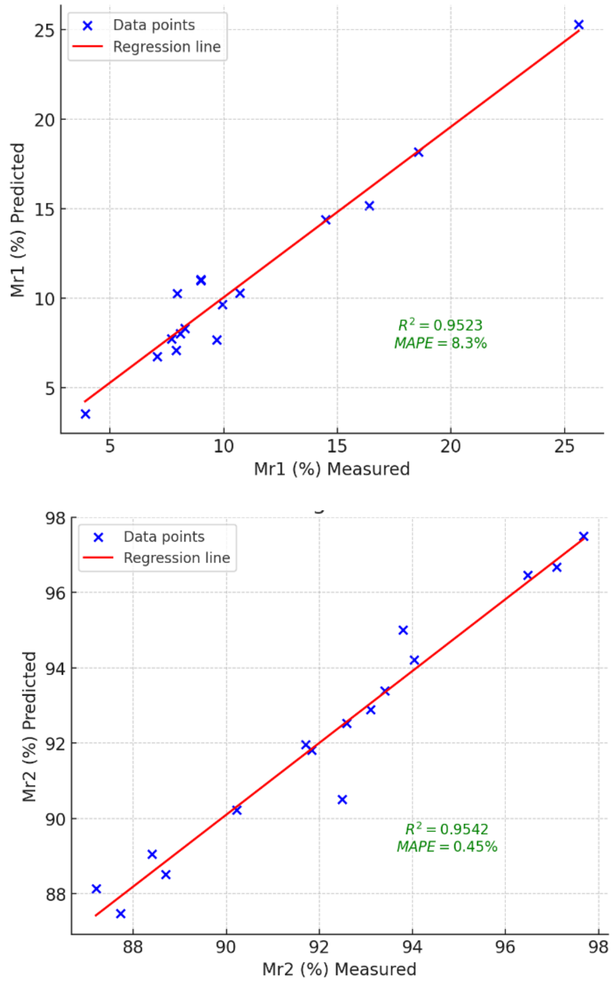

Fig. 10. Experimental and predicted results for the responses $Mr1$ and $Mr2$.

These responses include the reduced peak height (R_{pk}), core roughness depth (R_k), reduced valley depth (R_{vk}), as well as the material ratios in the peak and valley zones ($Mr1$ and $Mr2$). On the one hand, the strong correlation between these values confirms the robustness and reliability of the predictive model. On the other hand, significant deviations may indicate modeling limitations or experimental uncertainties. In this regard, most blue points overlap with the trendline, except for a few slightly deviating values. Furthermore, the coefficients of determination (R^2) for parameters R_{pk}, R_k, R_{vk}, $Mr1$, and $Mr2$ are 0.955, 0.959, 0.964, 0.952, and 0.954, respectively, while the mean absolute percentage errors (MAPE) are 8.48%, 6.86%, 5.75%, 8.3%, and 0.45%. Thus, all R^2 coefficients exceed the confidence threshold of 0.95, and all MAPE values remain below 10%, which demonstrates excellent model accuracy. Consequently, the reliable prediction of the five models is particularly important, especially in applications where surface properties affect the mechanical and tribological performance of materials.

3.3.2 3D response surface

Figures 11 to 15 present the 3D response surfaces for the Abbott–Firestone curve (BAC) parameters (R_{pk}, R_k, R_{vk}, $Mr1$, and $Mr2$), allowing for an examination of the most significant interaction effects among the model variables (V_c, f, ap, r_ε, and X_r). These interactions correspond to the most influential factors identified through analysis of variance and the Pareto diagram. The observed interactions are as follows: for the reduced peak height R_{pk} : V_c x f and f x X_r (Fig. 11); for the core roughness depth R_k : V_c x f and V_c x X_r (Fig. 12); for the reduced valley depth R_{vk} : V_c x f and V_c x X_r (Fig. 13); for the material ratio in the peak zone $Mr1$: f x ap and f x r_ε (Fig. 14); and for the material ratio in the valley zone $Mr2$: V_c x f and f x ap (Fig. 15).

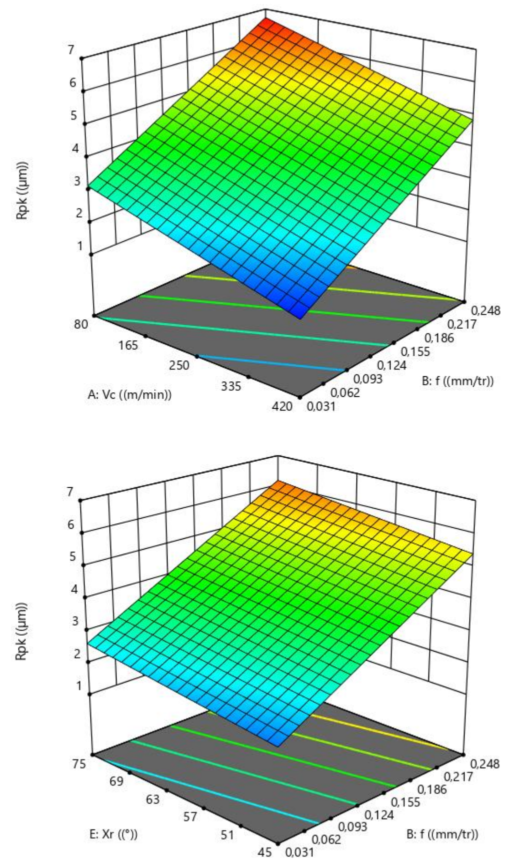

Fig. 11. 3D response surfaces for reduced peak height R_{pk} (V_c x f, f x X_r).

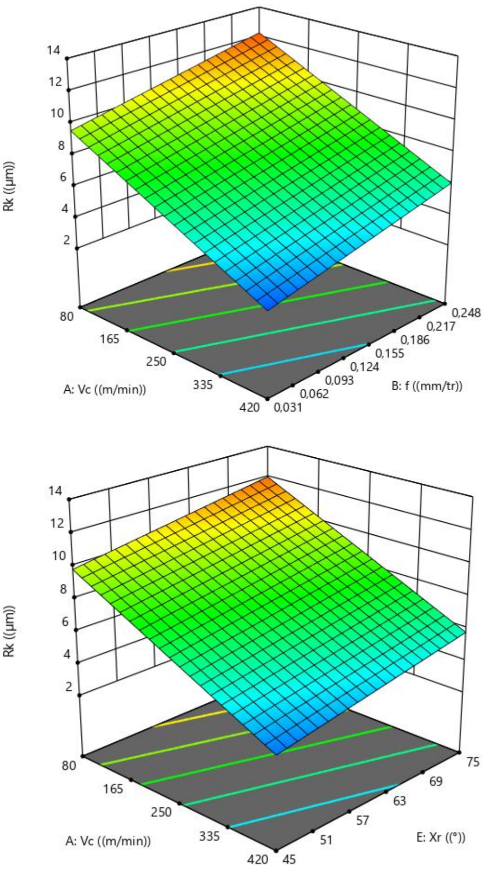

Fig. 12. 3D response surfaces for core roughness depth R_k (V_c x f, V_c x X_r).

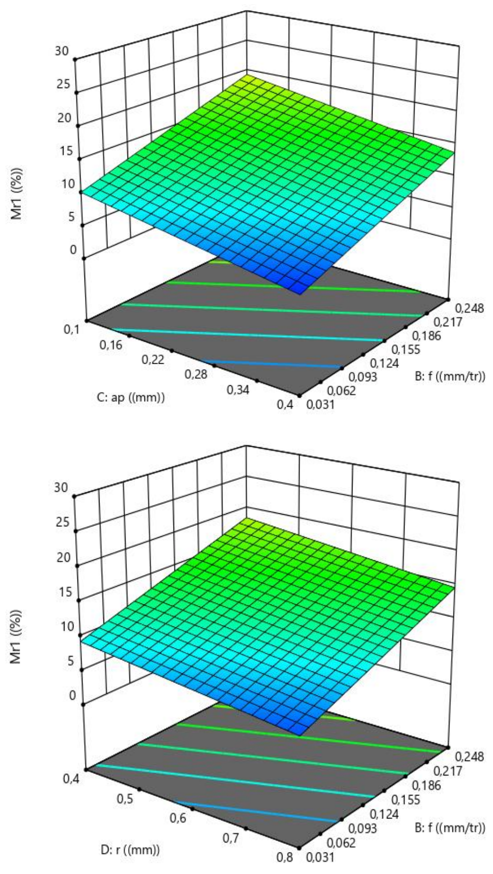

Fig. 14. 3D response surfaces for the peak material ratio $Mr1$ (f x ap, f x r_ε).

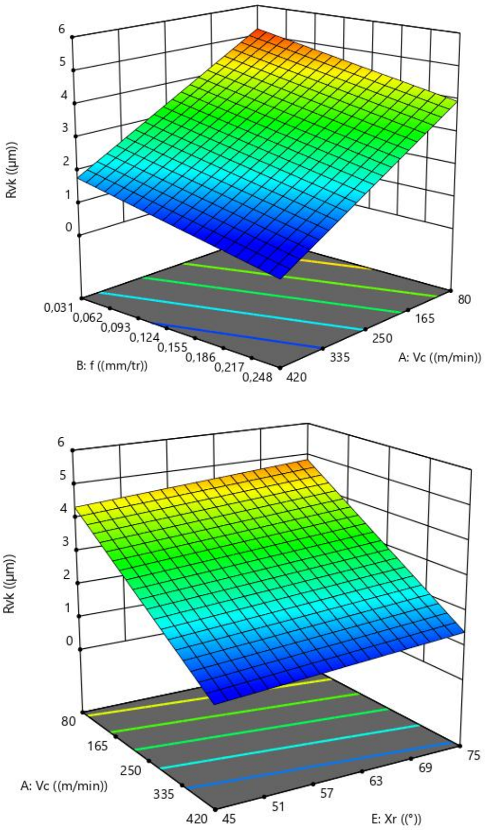

Fig. 13. 3D response surfaces for reduced valley depth R_{vk} (V_c x f, V_c x X_r).

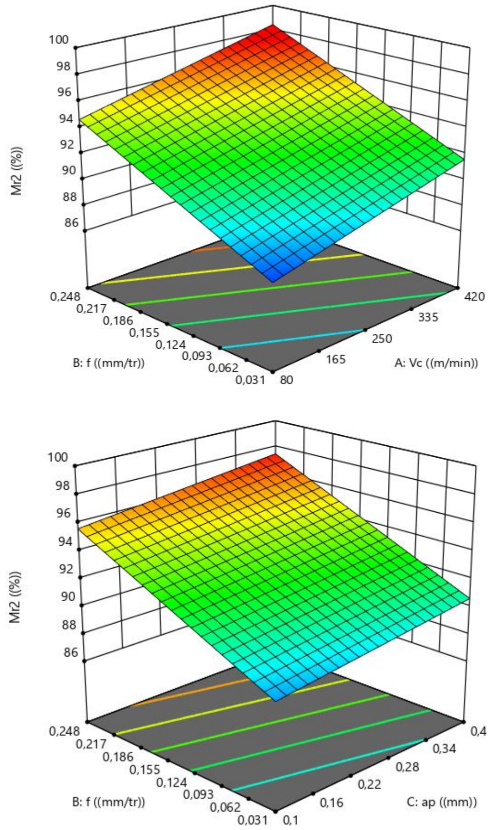

Fig. 15. 3D response surfaces for the valley material ratio $Mr2$ (V_c x f, f x ap).

Moreover, the unrepresented control factor is held constant at level 2 with the following values: V_c = 185 m/min, f = 0.062 mm/rev, ap = 0.2 mm, r_ε = 0.8 mm, and X_r = 75°. On one hand, the 3D visualization highlights the overall trends and response variations as a function of the influencing parameters, revealing regions where effects are more pronounced. A well-defined response surface with smooth transitions indicates good model stability, whereas irregularities or abrupt changes may suggest complex interactions or nonlinear effects.

According to Fig. 9, the feed (f) exhibits a steeper slope compared to the other two control factors (V_c and X_r), indicating that it is the primary factor influencing the peak height (R_{pk}). Next, the cutting speed (V_c) plays an important role, followed by the main cutting angle (X_r). Similarly, for the core roughness depth (R_k), V_c is the predominant factor, followed by f, and then X_r (Fig. 10). Moreover, these first two variables (V_c and f) also influence the depth of deep valleys (R_{vk}). However, unlike R_k, the tool radius (r_ε) is the third influencing factor for R_{vk} (see Fig. 11). Regarding the upper limiting position of the core roughness profile ($Mr1$), all factors are significant. However, f remains the most influential due to its steeper slope, followed by ap and r_ε (Fig. 12). Finally, the last response ($Mr2$) is influenced by the same parameters as R_{vk}, but with a different ranking for the first two factors: f leads, followed by V_c (Fig. 13).

The interaction patterns clearly confirm the dominant influence of feed (f) and speed (V_c) across most BAC parameters, with X_r and r_ε acting as secondary modifiers. In practical terms, a moderate feed rate (f ≈ 0.03–0.06 mm/rev) ensures a balanced compromise between peak height and material ratio stability, while maintaining cutting speed (V_c ≈ 180–280 m/min) helps reduce valley depth and enhances BAC quality without compromising tool life. A depth of cut (ap = 0.2–0.4 mm) and tool nose radius (r_ε = 0.8 mm) remain robust choices across responses, while a main cutting angle (X_r = 45–75°) provides flexibility to fine-tune interactions.

3.3.3 Experimental validation

Experimental validation is a crucial step in assessing the accuracy and relevance of the developed mathematical models. It involves comparing the predicted values generated by the model with the results obtained experimentally. In this context, three additional trials were carried out under cutting conditions different from those listed in Table 3. Furthermore, the absolute percentage error (APE) was calculated to objectively quantify the deviation between the experimental data and the predicted values. Table 4 shows the validation conditions and Table 5 shows their results.

Table 4. Validation conditions.

N°	V_C (m/min)	f (mm/tr)	ap (mm)	r_ε (mm)	X_r (°)
1	125	0,041	0,16	0,4	45
2	275	0,082	0,28	0,8	75
3	420	0,049	0,16	0,8	75

Table 5. Validation results.

N°	Experimental	RSM	APE (%)
(a) Reduced peak height ($\boldsymbol{R_{pk}}$)			
1	4,65	4,36	3,84
2	1,09	1,12	2,68
3	1,33	1,28	3,91
(b) Core roughness depth ($\boldsymbol{R_k}$)			
1	7,31	6,99	4,58
2	4,67	4,7	0,64
3	4,2	4,33	3,00
(c) Reduced valley depth ($\boldsymbol{R_{vk}}$)			
1	0,63	0,65	3,08
2	1,61	1,59	1,26
3	1,02	1	2,00
(d) Peak material ratio $\boldsymbol{Mr1}$ (%)			
1	14,39	13,75	4,65
2	7,54	7,84	3,83
3	8,54	8,25	3,52
(e) Valley material ratio $\boldsymbol{Mr2}$ (%)			
1	95,69	95,27	0,44
2	88,81	88,82	0,01
3	90,42	90,4	0,02

Table 5 reports the measured values, the predictions obtained from the RSM models, and the absolute percentage errors (APEs) for the five BAC output variables. The corresponding APE values were: reduced peak height (R_{pk}) – 2.68% and 3.91%; core roughness depth (R_k) – 0.64% and 4.58%; reduced valley depth (R_{vk}) – 1.26% and 3.08%; upper limit of the core material ratio

$Mr1$ (%) – 3.52% and 4.65%; and lower limit of the core material ratio $Mr2$ (%) – 0.01% and 0.44%. The highest recorded APE, 4.58%, reflects a very small deviation between experimental measurements and model predictions. This close agreement confirms the ability of the models to provide reliable estimations within the range of cutting conditions specified in Table 3.

3.4 Multi-objective optimization

In this section, both GRA and DF are employed for the optimization procedure. Each method is detailed below. In this regard, these two methods are the most widely used today.

3.4.1 Optimization using GRA

The grey relational analyze (GRA) evaluates many options in circumstances with little or confusing data. A gray relational coefficient determines how close each choice is to an ideal answer. This technique is frequently utilized in complex decision-making and multi-objective optimization problems [33–35].

GRA analysis uses different steps to evaluate and enhance alternatives among incomplete data. The process begins with the normalization of to render the data comparable within the [0, 1] interval. The phase considers the optimization criteria. An optimal solution is established as a factor for assessing alternatives, often given a value of 1.

The optimization of surface roughness—by reducing R_{pk}, R_k, and $Mr1$, and increasing $Mr2$ and R_{vk}—enhances the tribological performance of cylindrical surfaces by improving load-bearing capacity, and lubrication quality [30]. The results obtained after normalization are presented in Table 6. This table displays the experimental results, where all values have been scaled between 0 and 1. The row labeled "Ideal value" represents an optimal reference characterized by values equal to 1 across all criteria. Furthermore, each trial, numbered from 1 to 16, corresponds to an alternative evaluated based on multiple criteria. Thus, values close to 1 indicate high performance, whereas values close to 0 reflect poor performance. For example, Trial 13 stands out for its high performance across nearly all criteria, while Trial 16 is marked by several zero.

Table 6. Normalized experimental results ($\boldsymbol{x_i}$ $(\boldsymbol{k})$).

Trail n°	R_{pk}	R_k	R_{vk}	$Mr1$	$Mr2$
Ideal value	1.000	1.000	1.000	1.000	1.000
1	0.703	0.393	0.968	0.798	0.051
2	0.638	0.427	0.834	0.825	0.115
3	0.237	0.091	0.721	0.733	0.505
4	0.000	0.000	0.789	0.766	0.630
5	0.690	0.325	0.948	0.816	0.000
6	0.566	0.179	1.000	0.687	0.143
7	0.600	0.674	0.299	0.808	0.592
8	0.050	0.433	0.224	0.424	0.946
9	0.781	0.662	0.454	0.814	0.288
10	0.717	0.707	0.320	0.721	0.442
11	0.606	0.453	0.549	0.766	0.430
12	0.409	0.528	0.290	0.513	0.886
13	1.000	1.000	0.109	1.000	0.515
14	0.977	0.951	0.061	0.854	0.564
15	0.676	0.866	0.045	0.325	0.653
16	0.201	0.406	0.000	0.000	1.000

Table 7. Grey relational coefficients ($\boldsymbol{\eta_i}$ $(\boldsymbol{k})$).

Trail n°	GRC η_i (k)					GRG (α_i)	
	R_{pk}	R_k	R_{vk}	$Mr1$	$Mr2$	α_i	Ordre
1	0.627	0.452	0.940	0.712	0.345	0.615	3
2	0.580	0.466	0.751	0.741	0.361	0.580	6
3	0.396	0.355	0.642	0.652	0.503	0.510	15
4	0.333	0.333	0.703	0.681	0.575	0.525	13
5	0.617	0.425	0.906	0.731	0.333	0.602	4
6	0.536	0.379	1.000	0.615	0.369	0.580	7
7	0.556	0.605	0.416	0.722	0.551	0.570	8
8	0.345	0.469	0.392	0.465	0.902	0.515	14
9	0.696	0.597	0.478	0.728	0.413	0.582	5
10	0.638	0.630	0.424	0.642	0.473	0.561	9
11	0.559	0.477	0.526	0.681	0.467	0.542	11
12	0.458	0.515	0.413	0.507	0.815	0.542	12
13	1.000	1.000	0.359	1.000	0.508	0.773	1
14	0.955	0.911	0.348	0.774	0.534	0.704	2
15	0.607	0.789	0.344	0.426	0.591	0.551	10
16	0.385	0.457	0.333	0.333	1.000	0.502	16

The values of the grey relational coefficients (GRC) are presented in Table 7. This table shows the coefficients obtained after comparison with the ideal solution. These coefficients assess the closeness of each alternative to the reference. The closer a coefficient is to 1, the more similar the alternative is to the ideal solution.

Conversely, a lower coefficient indicates a greater deviation. For instance, Trial 13 displays the highest coefficients, confirming its strong proximity to the optimal solution.

The grey relational grades (α_i) are presented in Table 7. This table aggregates the grey relational coefficients of each trial into a single grey relational grade, thereby facilitating the ranking of alternatives. A higher GRG indicates better overall performance of the corresponding trial. Consequently, the trials are ranked from best to worst. Trial 13 ranks first with the highest GRG (0.773), while Trial 16 ranks last with the lowest GRG (0.502).

The GRG (α_i) identified Trial 13 as the best alternative based on the evaluated criteria. This ranking proves particularly useful for optimization, as it facilitates the selection of the most suitable parameters in contexts with partially known information. The optimal combination of cutting parameters is presented in Table 7. It is defined as follows: cutting speed at level 4, feed at level 1, depth of cut at level 4, nose radius at level 2, and principal cutting angle at level 1. Therefore, the optimal combination for the five responses is represented as: V_c-4f-1ap-4r_ε-2X_r-1. The corresponding optimal cutting parameter values are: V_c = 420 m/min, f = 0.031 mm/rev, ap = 0.4 mm, r_ε = 0.8 mm, and X_r = 45°.

3.4.2 Optimization using DF

The desirability function (DF) is a multi-criteria optimization method that converts several responses into a single overall value, facilitating the comparison and selection of the best alternative. Each criterion is normalized on a scale from 0 (unacceptable) to 1 (ideal), depending on whether the objective is to maximize, minimize, or target a specific value. These desirability indices are then combined using a weighted geometric mean, allowing the relative importance of each criterion to be considered. The solution with the highest overall desirability is selected as optimal. Widely applied in industrial optimization, product design, and decision-making, this approach has been employed with response surface methodology (RSM) by researchers such as Pradhan et al. [36], Şahin et al. [37], and Al Njjar et al. [38].

The objective of this study is to optimize the cutting conditions during the turning of C45 steel using the desirability function (DF). This optimization aims to minimize certain output parameters (R_{pk} ↘, R_k ↘, and $Mr1$ ↘), while maximizing others (R_{vk} ↗ and $Mr2$ ↗).). The analysis is based on Tables 8 and 9, and Fig. 16. Table 8 defines the limits of the cutting parameters as well as the optimization goals for each response. Consequently, Table 9 presents the optimal cutting parameters.

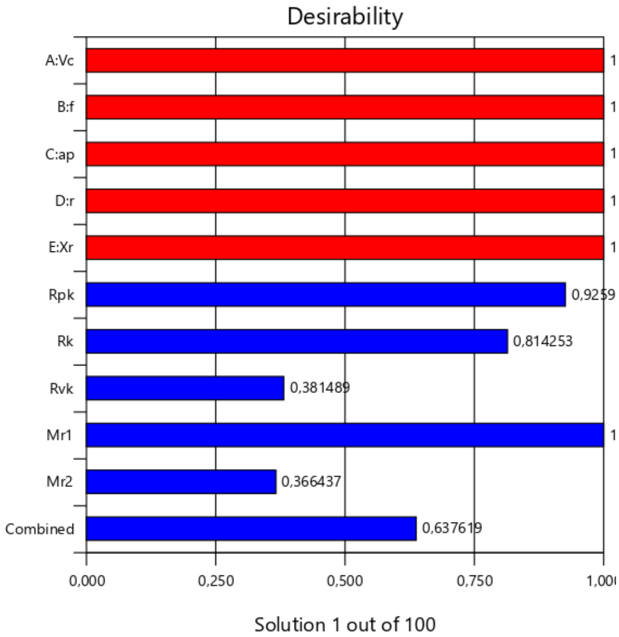

Fig. 16. Analog bars of the individual desirability.

Table 8. Optimization constraints.

Conditions	Goal	Lower limit	Upper limit
V_c (m/min)	In range	80	420
f (mm/rev)	In range	0.031	0.248
ap (mm)	In range	0.1	0.4
r_ε (mm)	In range	0.4	0.8
X_r (°)	In range	45	75

Combined optimization ensures high-quality Abbott–Firestone curve parameters, which is particularly valuable in the automotive sector. As shown in Fig. 16, the individual desirability indices and their contribution to the overall DF indicate a stable combined desirability of about 0.637–0.638, confirming the robustness of the optimization. According to Table 9 and Fig. 16, the optimal cutting parameters for improving BAC quality are $V_c = 278{,}47\ m/min$, $f = 0{,}033\ mm/tr$, $ap = 0{,}4\ mm$, $r_\varepsilon = 0{,}8\ mm$, and

$X_r = 45°$. Under these conditions, the BAC parameters are $R_{pk} = 1{,}61\ \mu m$, $R_k = 4{,}46\ \mu m$, $R_{vk} = 2{,}70\ \mu m$, $Mr1 = 1{,}66\%$, and $Mr2 =$ 91,03%. Notably, the lower R_pk compared to R_vk, in line with Feng et al. [39], indicates a surface free from sharp peaks.

Table 9. Optimization of the five responses.

N°	V_c	f	ap	r_ε	X_r	R_{pk} (µm)	R_k (µm)	R_{vk} (µm)	$Mr1$ (%)	$Mr2$ (%)	DF
1	278.47	0.033	0.40	0.8	45	1.61	4.46	2.70	1.66	91.03	0.638
2	280.06	0.034	0.39	0.8	45	1.61	4.46	2.69	1.74	91.05	0.638
3	275.68	0.038	0.40	0.8	45	1.70	4.57	2.70	1.81	91.14	0.638
4	283.68	0.033	0.40	0.8	45	1.57	4.36	2.65	1.71	91.08	0.638
5	273.97	0.037	0.39	0.8	45	1.69	4.60	2.73	1.76	91.08	0.638
6	275.93	0.039	0.40	0.8	45	1.72	4.58	2.69	1.86	91.18	0.638
7	283.27	0.033	0.39	0.8	45	1.59	4.43	2.68	1.87	91.04	0.637
8	286.02	0.032	0.40	0.8	45	1.55	4.31	2.63	1.72	91.08	0.637
9	281.66	0.036	0.39	0.8	45	1.64	4.51	2.69	1.98	91.08	0.637
10	269.39	0.039	0.40	0.8	45	1.75	4.70	2.76	1.78	91.12	0.637

• The values in bold indicate the chosen optimal cutting parameters, providing the best responses.

A comparison of the optimal cutting conditions obtained with the two optimization methods reveals both similarities and differences. Using GRA, the optimal parameters were V_c = 420 m/min, f = 0.031 mm/rev, ap = 0.4 mm, r_ε = 0.8 mm, and X_r = 45°, whereas the DF method, targeting improved Abbott–Firestone curve quality, yielded $V_c = 278{,}47\ m/min$, $f = 0{,}033\ mm/tr$, $ap = 0{,}4\ mm$, $r_\varepsilon = 0{,}8\ mm$, and $X_r = 45°$. The two methods provided identical values for the depth of cut, tool nose radius, and principal cutting angle, while the feed rate differed only marginally. The main divergence lies in the cutting speed, with GRA favoring a significantly higher value, reflecting its multi-response optimization strategy, and DF selecting a lower value that favors BAC-related surface characteristics. These results suggest that the choice between the two solutions should depend on whether the primary objective is overall process performance (GRA) or enhanced BAC quality (DF). Moreover, from a practical standpoint, the DF-derived cutting speed falls within typical industrial ranges, which may contribute to extended tool life and reduced machining costs, thereby reinforcing its feasibility for real-world applications.

4. CONCLUSIONS

The objective of this study is to simultaneously optimize the cutting conditions (V_c, f, ap, r_ε, and X_r) to improve the quality of the bearing area curve parameters ($\min R_{pk}$, $\min R_k$, $max\ R_{vk}$, $min\ Mr1$, and $max\ Mr2$). This dual optimization enables the identification of ideal cutting conditions while addressing the specific targets for each parameter: minimizing R_{pk}, R_k, and $Mr1$, and maximizing R_{vk} and $Mr2$. The main conclusions drawn from this study are as follows:

- The examination of surface topography by BAC characteristics offers a more precise characterization than traditional roughness metrics (Ra, Rz). The BAC characteristics are crucial for assessing the tribological performance of surfaces, particularly for components enduring high loads and necessitating efficient lubricant retention.
- The Pareto diagrams indicate that f and V_c are the most significant factors affecting the five BAC criteria (R_{pk}, R_k, R_{vk}, $Mr1$, and $Mr2$). A decreased feed rate decreases peak roughness, whilst an elevated cutting speed fosters valley development, thus enhancing lubricant retention. Conversely, ap, X_r, and r_ε have a secondary but significant function and may be modified with more freedom.
- Linear regression effectively represented the influence of cutting parameters on the bearing curve indicators, achieving determination coefficients (R^2) over 95% and mean absolute percentage errors (MAPE) below 10%.

- The use of the GRA approach and DF facilitated the identification of optimal cutting settings for machining C45 steel. The findings indicate that an elevated cutting speed (Vc = 420 m/min), a minimal feed rate (f = 0.031 mm/rev), and a maximum depth of cut (ap = 0.4 mm), in conjunction with an extensive nose radius ($r\varepsilon$ = 0.8 mm) and a diminished primary cutting angle (Xr = 45°), enhance the process efficiency. A GRG index of 0.773 and a constant DF value of around 0.638 indicate strong and consistent optimization. Under this cutting regime, the BAC characteristics are as follows: Rpk = 1.61 μm, Rk = 4.46 μm, Rvk = 2.70 μm, $Mr1$ = 1.66%, and $Mr2$ = 91.03%.
- Future work will focus on integrating minimum quantity lubrication (MQL), the use of nanofluids, and vegetable oils to investigate their effect on the values and functionalities of BAC parameters.

REFERENCES

[1] A. la Monaca et al., "Surface integrity in metal machining - Part II: Functional performance," *International Journal of Machine Tools and Manufacture*, vol. 164, p. 103718, May 2021, doi: 10.1016/j.ijmachtools.2021.103718.

[2] M. Sarıkaya et al., "A state-of-the-art review on tool wear and surface integrity characteristics in machining of superalloys," *CIRP Journal of Manufacturing Science and Technology*, vol. 35, pp. 624–658, Nov. 2021, doi: 10.1016/j.cirpj.2021.08.005.

[3] M. Praniewicz et al., "Bearing area curve-based partitioning for the verification of theoretical supplemental geometry on additively manufactured lattice structures," *Additive Manufacturing*, vol. 68, p. 103521, Apr. 2023, doi: 10.1016/j.addma.2023.103521.

[4] Y. Lü et al., "3D Roughness Prediction Modeling and Evaluation of Textured Liner of Piston Component-Cylinder System," *Chin. J. Mech. Eng*, vol. 37, no. 1, , pp. 1–13, Aug. 2024, doi: 10.1186/s10033-024-01089-3.

[5] *Geometrical product specifications (GPS) — Surface texture: Profile — Part 2: Terms, definitions and surface texture parameters*, ISO 21920-2, 2021.

[6] I. Buj-Corral and J. Vivancos-Calvet, "Roughness variability in the honing process of steel cylinders with CBN metal bonded tools," *Precis En*, vol. 35, no. 2, pp. 289–293, Apr. 2011, doi: 10.1016/j.precisioneng.2010.11.004.

[7] L. J. Arantes et al, "The roughness characterization in cylinders obtained by conventional and flexible honing processes," *The International Journal of Advanced Manufacturing Technology*, vol. 93, 635–649 pp. 1–14, Mar. 2017, doi: 10.1007/s00170-017-0544-2.

[8] V. Nagandran, T. V. Janahiraman, and N. Ahmad, "Modeling and Optimization of Carbon Steel AISI 1045 Surface Roughness in CNC Turning Based on Response Surface Methodology and Heuristic Optimization Algorithms," *American Journal of Neural Networks and Applications*, vol. 3, no 6, pp. 56-62, Dec. 2017, doi: 10.11648/j.ajnna.20170306.11.

[9] E. Feldshtein et al., "The Influence of the Conditions of Emulsion Mist Formation on the Surface Roughness of AISI 1045 Steel After Finish Turning," *Advances in Science and Technology Research Journal*, vol. 10, no. 30, pp. 144–149, Jun. 2016, doi: 10.12913/22998624/62773.

[10] A. T. Abbas et al., "Multi-Objective Optimization of Performance Indicators in Turning of AISI 1045 under Dry Cutting Conditions," *Metals*, vol. 13, no. 1, p. 96, Jan. 2023, doi: 10.3390/met13010096.

[11] A. T. Abbas et al, "Effects of Tool Edge Geometry and Cutting Conditions on the Performance Indicators in Dry Turning AISI 1045 Steel," *Machines*, vol. 11, no. 3, p. 397, Jan. 2023, doi: 10.3390/machines11030397.

[12] N. Szczotkarz et al., "Formation of Surface Topography During Turning of AISI 1045 Steel Considering the Type of Cutting-Edge Coating," *Advances in Science and Technology Research Journal*, vol. 15, no. 4, pp. 253–266, Dec. 2021, doi: 10.12913/22998624/141991.

[13] H. Klippel et al., "Large-scale investigation of dry orthogonal cutting experiments Ti6Al4V and Ck45," *The International Journal of Advanced Manufacturing Technology*, vol. 135, no. 5-6, pp. 2871–2908, Nov. 2024, doi: 10.1007/s00170-024-14597-2.

[14] A. T. Abbas et al., "Effect of Wiper Edge Geometry on Machining Performance While Turning AISI 1045 Steel in Dry Conditions Using the VIKOR-ML Approach," *Machines*, vol. 11, no. 7, p. 719, Apr. 2023, doi: 10.3390/machines11070719.

[15] J. Jurko et al., "Optimization of Sustainable Production Processes in C45 Steel Machining Using a Confocal Chromatic Sensor," *Lubricants*, vol. 12, no. 3, p. 99, Mar. 2024, doi: 10.3390/lubricants12030099.

[16] L. W. Hernández González et al., "Selection of Machining Parameters Using a Correlative Study of Cutting Tool Wear in High-Speed Turning of AISI 1045 Steel," *Journal of Manufacturing and Materials Processing*, vol. 2, no. 4, p. 66, Dec. 2018, doi: 10.3390/jmmp2040066.

[17] N. Puneeth Kumar et al., "Performance and Comparison of Coated and Uncoated Tool Inserts in Machining of C45 Steel," *Journal of Mines, Metals and Fuels*, vol. 70, no. 10, pp. 116-122, Oct. 2022, doi: 10.18311/jmmf/2022/31210.

[18] L. C. Magalhães et al., "Tool Wear Effect on Surface Integrity in AISI 1045 Steel Dry Turning," *Materials*, vol. 15, no. 6, p. 2031, Mar. 2022, doi: 10.3390/ma15062031.

[19] M. Kuruc et al., "The Influence of Cutting Parameters on Plastic Deformation and Chip Compression during the Turning of C45 Medium Carbon Steel and 62SiMnCr4 Tool Steel," *Materials*, vol. 15, no. 2, p. 585, Jan. 2022, doi: 10.3390/ma15020585.

[20] A. Dabwan et al., "Integrating an artificial neural network with genetic, particle swarm optimization algorithms, and fuzzy rule to optimize the surface roughness in dry turning AISI 1045 steel," *Mater. Res. Express*, vol. 12, pp. 1–19, Jul. 2025, doi: 10.1088/2053-1591/adf41b.

[21] B. Sredanovica et al., "Multi-Objective Optimization of Sustainable Steel AISI 1045 Turning Energy Parameters Under MQL Condition," *Tribology in Industry*, vol. 44, no. 3, pp. 498-507, Sep. 2022, doi: 10.24874/ti.1301.05.22.07.

[22] *Geometrical product specifications (GPS)– surface texture: profile method– motif parameters*, ISO 12085, 1996.

[23] S. S. Kallesh and R. N. Marigoudar, "Taguchi Method for Tribological Excellence: Insights into Copper-Based Metal Matrix Composites," *Tribology in Industry*, vol. 47, no. 2, pp. 279-293, Jun. 2025, doi: 10.24874/ti.1841.12.24.03.

[24] S. Kumar, S. K. Ghosh, and N. N. Pawar, "Design of Experiment with Tribological Performance Analysis of Electroless Nano-composite Ni-P-SiC Coating for Conveyors," *Tribology in Industry*, vol. 44, no. 4, pp. 707-718, Dec. 2022, doi: 10.24874/ti.1371.09.22.11.

[25] A. Hamdi, Y. F. Yapan, A. Uysal, and H. Abderazek, "Multi-objective analysis and optimization of energy aspects during dry and MQL turning of unreinforced polypropylene (PP): an approach based on ANOVA, ANN, MOWCA, and MOALO," *The International Journal of Advanced Manufacturing Technology*, vol. 128, no. 11–12, pp. 4933–4950, Sep. 2023, doi: 10.1007/s00170-023-12205-3.

[26] G. P. Petropoulos, C. N. Pandazaras, and J. P. Davim, "Surface texture characterization and evaluation related to machining," in *Springer eBooks*, 2010, pp. 37–66. doi: 10.1007/978-1-84882-874-2_2.

[27] A. Hamdi et al., "Investigation of MQL and CNC turning parameters on the machinability of unreinforced polypropylene: study of surface roughness, temperature, and specific cutting energy," *The International Journal of Advanced Manufacturing Technology*, vol. 130, no. 1-2, pp. 717–730, Jan. 2024, doi: 10.1007/s00170-023-12761-8.

[28] T. Hakmi et al., "Machinability investigation during turning of polyoxymethylene POM-C and optimization of cutting parameters using Pareto analysis, linear regression and genetic algorithm," *Archive of Mechanical Engineering*, vol. 71, no, 1, pp. 47–71, Mar. 2024, doi: 10.24425/ame.2024.149184

[29] A. Hamdi et al., "Machinability assessment and optimization of turning AISI H11 steel under various minimum quantity lubrication (MQL) conditions using nanofluids," *The International Journal of Advanced Manufacturing Technology*, vol. 137, no. 7-8, pp. 4089–4107, Mar. 2025, doi: 10.1007/s00170-025-15418-w.

[30] L. C. Pereira et al., "Assessment of the effect of cutting parameters on roughness in flexible honed cylinders," *The International Journal of Advanced Manufacturing Technology*, vol. 95, no,1-4, pp. 181–196, Mar. 2018, doi: 10.1007/s00170-017-1200-6.

[31] M. A. Chowdhury et al., "Analysis and Optimization of Turned Surfaces of AISI 1060 using ANOVA and Regression," *Tribology in Industry*, vol. 41, no. 1, pp. 23-32, Mar. 2019, doi: 10.24874/ti.2019.41.01.03.

[32] I. Peko et al., "Modeling of Surface Roughness in Plasma Jet Cutting Process of Thick Structural Steel," *Tribology in Industry*, vol. 38, no. 4, pp. 522-529, Dec. 2016.

[33] R. Kumar et al, "Investigation on Tool Wear and Surface Characteristics in Hard Turning Under Air-Water Jet Spray Impingement Cooling Environment," *Tribology in Industry*, vol. 41, no. 2, pp. 172-187, Jun. 2019, doi: 10.24874/ti.2019.41.02.04.

[34] S. K. Pradhan, R. Kumar, and P. C. Mishra, "Computer Simulation and Optimization of Elliptic Bore Journal Bearing," *Tribology in Industry*, vol. 44, no. 2, pp. 322-333, Jun. 2019, doi: 10.24874/ti.1179.09.21.01.

[35] T. Hakmi et al, "Mathematical modeling using ANN based on k-fold cross validation approach and MOAHA multi-objective optimization algorithm during turning of polyoxymethylene POM-C," *Jordan Journal of Mechanical and Industrial Engineering*, vol. 18, no. 1, pp. 179–190, Mar. 2024, doi: 10.59038/jjmie/180114.

[36] S. K. Pradhan, A. Gupta, and P. C. Mishra, "Investigating into the Effects of Bore Irregularities on the Hydrodynamic Performance Journal Bearing Using Response Surface Methodology," *Tribology in Industry*, vol. 24, no. 2, pp. 201-211, Jun. 2023, doi: 10.24874/ti.1431.01.23.03.

[37] Y. Şahin, A. Deniz, and F. Şahin, "Investigation of Abrasive Wear Performances of Different Polyamides by Response Surface Methodology," *Tribology in Industry*, vol. 31, no. 3, pp. 321-329, Sep. 2019, doi: 10.24874/ti.2019.41.03.02.

[38] A. Al Njjar, K. Mazloum, and A. Sata, "Fabrication and Characterization of Physical, Mechanical, and Wear Characteristics of AA7075/SiC Composites by Floating Die," *Tribology in Industry*, vol. 46, no. 4, pp. 596-610, Dec. 2024, doi: 10.24874/ti.1672.04.24.07.

[39] C. X. Feng, X. Wang, and Z. Yu, "Neural networks modeling of honing surface roughness parameters defined by ISO 13565," *Journal of Manufacturing Systems*, vol. 21, no. 5, pp. 395–408, Oct. 2002, doi: 10.1016/S0278-6125(02)80037-1.